Available online at www.sciencedirect.com
SCIENCE DIRECT®
International Journal of Heat and Mass Transfer 49 (2006) 1090–1099
International Journal of HEAT and MASS TRANSFER
www.elsevier.com/locate/ijhmt

Optimization of micro heat exchanger: CFD, analytical approach and multi-objective evolutionary algorithms

Kwasi Foli [a,1], Tatsuya Okabe [b], Markus Olhofer [b], Yaochu Jin [b], Bernhard Sendhoff [b,*]

[a] Honda Research Institute USA Inc., 1381 Kinnear Road, Columbus, OH 43212, USA
[b] Honda Research Institute Europe GmbH, Carl-Legien-Strasse 30, D-63073 Offenbach/M, Germany

Received 12 April 2005; received in revised form 8 August 2005
Available online 25 October 2005

Abstract

Advances in miniaturization have led to the use of microchannels as heat sinks in industry. Studies have established that the thermal performance of a microchannel depends on its geometric parameters and flow conditions. This paper describes two approaches for determining the optimal geometric parameters of the microchannels in micro heat exchangers. One approach combines CFD analysis with an analytical method of calculating the optimal geometric parameters of micro heat exchangers. The second approach involves the usage of multi-objective genetic algorithms in combination with CFD.

Keywords: Computational fluid dynamics; Micro heat exchanger; Optimization; Multi-objective; Optimal shape; Evolutionary algorithms

1. Introduction

The trend toward miniaturization and the advances in microfabrication have led to the application of microchannels for thermal management in areas such as medicine, consumer electronics, avionics, metrology, robotics, process industry, telecommunication and automotive industries to mention just a few. Since the work of Tuckerman and Pease [1], microchannels have received considerable attention particularly in the areas of experimental [2–10], analytical [11–19] and numerical [10,20–23] studies. These studies revealed deviations in the heat transfer and fluid flow characteristics in microscale devices from those of conventionally-sized (or macro-scale) devices. The flow and heat transfer characteristics of fluids flowing in microchannels could not be adequately predicted by the theories and correlations developed for conventionally-sized channels. The studies [15,16] further showed that the performance of a microchannel heat exchanger depends very much on the aspect ratio (AR) of the channels. Bau [24] conducted optimization studies to minimize temperature gradient and overall thermal resistance in microchannels and concluded that reduction in overall thermal resistance could be achieved by varying the cross-sectional dimensions of a microchannel.

In spite of the widespread use of micro heat exchangers (μHEXs) in the process and automotive industries, there is limited published literature on attempts at designing them for optimal performance.

The objective of this paper is to present two methods for determining the optimal design parameters of the microchannels in μHEXs that maximize the heat transfer rate (or heat flux) subject to specified design constraints. The first is a simple approach that combines CFD with the analytical solution of a simplified transport equation for momentum and heat transfer. This approach optimizes the dimensions of a microchannel with predetermined geometry. The second approach, a more sophisticated method, not only determines the optimal dimensions of a heat exchanger but also determines the optimum shape

* Corresponding author.
E-mail addresses: Kwasi.Foli@SARTORIUS.com (K. Foli), tatsuya_okabe@n.w.rd.honda.co.jp (T. Okabe), bs@honda-ri.de (B. Sendhoff).
[1] Present address: Sartorius AG, Weender Landstrasse 94-108, D-37075 Göttingen, Germany.

0017-9310/$ - see front matter © 2005 Elsevier Ltd. All rights reserved.
doi:10.1016/j.ijheatmasstransfer.2005.08.032

Nomenclature

b	length scale as defined in Eq. (5)
c_p	specific heat capacity at constant pressure
d_h	hydraulic diameter
g	acceleration due to gravity
h	heat transfer coefficient, specific enthalpy (in Eq. (3))
H	height of microchannels
k	thermal conductivity
l	length of channel
Nu	Nusselt number
u_i	velocity component in tensor notation
p	pressure
ΔP (ΔP_h, ΔP_c)	pressure drop (hot, cold gas channel)
s	thickness of material separating channels (Table 2)
T	temperature
x_i	general coordinate direction
w	width of channel
Q	heat transfer

Greek symbols

α	ratio in Eq. (7)
β	bulk viscosity
δ_{ij}	Kronecker delta function
μ	dynamic viscosity
ρ	density
τ_{ij}	stress tensor

Subscripts

c	channel
f	fluid
s	solid

based on imposed operating conditions. This approach increases the degree of freedom of the geometrical variations by combining CFD analyzes with multi-objective evolutionary algorithms (MOEAs).

2. Mathematical model

The problem under consideration is the forced convection through μHEX. A schematic model of the μHEX is shown in Fig. 1. It consists of rectangular channels with hot and cold fluid flowing through alternate channels. The dimensions of the heat exchanger core are shown in the figure. The method described here applies to both co- and counter-flow configurations.

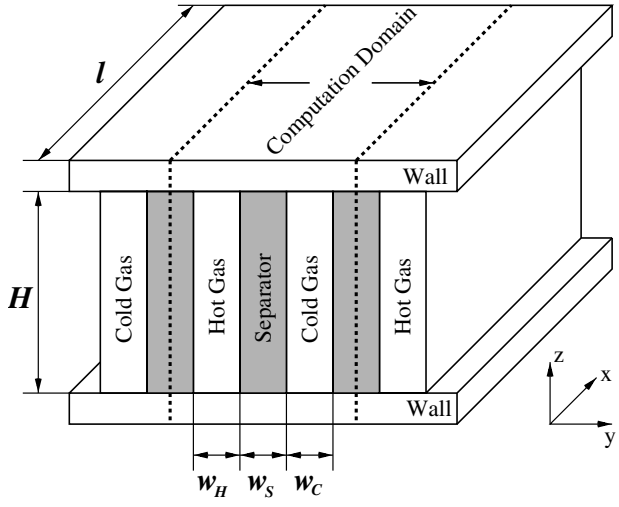

Fig. 1. A schematic model of the micro heat exchanger. The micro heat exchanger consists of three parts, i.e., a hot gas channel, a cold gas channel and a separator. The heat energy in the hot gas channel will be transferred to the cold gas channel via the separator.

For the studies reported in this paper, the hydraulic diameter of microchannels considered was between 100 μm and 1000 μm. The Knudsen number for all the flows considered was less than 0.001, a necessary condition for continuum flow. Therefore, the conservation equations based on continuum flow apply. The governing equations that describe the steady state momentum and heat are given in tensor notations below.

Continuity and momentum

$$\frac{\partial}{\partial x_i}(\rho v_i) = 0, \quad \rho u_j \frac{\partial u_i}{\partial x_j} = -\frac{\partial p}{\partial x_i} + \rho g_i + \frac{\partial \tau_{ij}}{\partial x_j}, \quad \text{where}$$
$$\tau_{ij} = \mu\left(\frac{\partial u_i}{\partial x_j} + \frac{\partial u_j}{\partial x_i}\right) + \left(\beta - \frac{2}{3}\mu\right)\frac{\partial u_k}{\partial x_k}\delta_{ij}. \tag{1}$$

Energy

$$\rho u_j \frac{\partial h}{\partial x_i} = u_i \frac{\partial p}{\partial x_i} + \phi + \frac{\partial}{\partial x_i}\left(k\frac{\partial T}{\partial x_i}\right), \quad \text{where } \phi = \tau_{ij}\frac{\partial u_i}{\partial x_j}. \tag{2}$$

In steady state the conservation equations are written in the general form

$$\frac{\partial}{\partial x_i}(\rho u_i \phi) = \frac{\partial}{\partial x_i}\left(\Gamma \frac{\partial \phi}{\partial x_i}\right) + S, \tag{3}$$

where ϕ represents a general dependent variable such as velocity or temperature, Γ is a diffusion coefficient and S is a source term. The partial differential equations represented in general by Eq. (3) were discretized over spatial coordinates by means of the control volume technique [25]. To predict the thermal performance of the μHEX the resulting finite difference equations were solved in three-dimensions using an iterative, segregated solution method wherein the

equation sets for each dependent variable were solved sequentially till a preset convergence criterion was satisfied. The SIMPLEC solution algorithm [26] was used to treat the pressure–velocity coupling of the flow field. To ensure faster convergence of the equations, an Algebraic Multigrid solver [27] was used for each of the resulting algebraic finite difference equations. The set of equations were solved using a commercial CFD software, CFD-ACE+ [28] that incorporates the aforementioned equation solver and solution strategy. In solving the transport equations, the Dirichlet boundary conditions were set for the mass flow rate and temperature of the fluids at the inlet boundaries, while the Naumann boundary conditions were specified for the temperature and velocity components at the outlet boundaries of the computational domains. Adiabatic boundary conditions were imposed on the walls and the continuity of the temperature and heat flux was used as the conjugate boundary conditions to couple the energy equations for the solid and fluid phases. The no-slip boundary condition was imposed on the velocity components at the wall. Finally, the ideal-gas law was used to calculate the thermodynamics properties of the gases in the study. Since geometric periodicity exists in the cases studied the computational domain is simplified as shown marked in Fig. 1.

In performing the simulation the computational domain was populated with structured (hexahedral) cells. For each study, a grid-independent solution was achieved and the number of cells depended on the aspect ratio that was investigated. Typically, a grid-independent solution was achieved for the lower aspect ratio cases with about 43,500 cells. With a convergence criterion set at 0.0001, convergence was attained at an average time of 1440 CPU seconds.

3. Optimization

3.1. Analytical approach combined with CFD

The optimal geometric parameters of the channels of a μHEX are determined using a combination of CFD and the analytical approach of Samalam [12]. Samalam reduced the analysis of the microchannel flow problem to a quasi two-dimensional differential equation and presented exact solutions to analytically determine the optimal dimensions of microchannels under given constraints. Based on the given constraints such as pumping power and space limitation the variables to be optimized are the channel width, aspect ratio and channel spacing. The optimal aspect ratio of the μHEX channels, subject to the constraints imposed, was determined using CFD. As will be explained later, based on the problem specification, the optimal geometric parameters of a microchannel are either directly obtained based on the determined optimal aspect ratio or these are calculated by combining the optimal aspect ratio with the relationships derived by Samalam.

The first step towards the optimization was to determine the performance characteristics of the μHEX by numerically solving the conservation equations. The two design scenarios considered were: (1) the allowable volume of the heat exchanger was fixed based on design constraints; (2) no limit was placed on the volume of the μHEX core. However, the dimensions of the microchannels were within the limits defined for a μHEX. For both cases, Inconel with a thickness of 0.1 mm was the material of the μHEX; nitrogen was used as the hot fluid and carbon dioxide as the coolant.

3.1.1. Determination of the optimal aspect ratio for constant volume of microchannels

This situation applies to cases where the volume of the μHEX is fixed by design considerations. In the study presented in this paper, each microchannel of the heat exchanger was assigned a volume of 50 mm^3. Assuming a fixed length of 40 mm for all channels, this resulted in a constant cross-sectional area of 1.25 mm^2 for each microchannel. For the analysis, the aspect ratio, AR, of a channel, was defined as the ratio of height of channel to its width, i.e.,

$$\mathrm{AR} = \frac{H}{w_c}. \tag{4}$$

Numerical simulations were performed by varying the aspect ratio of the microchannels in the range $1.25 \leqslant \mathrm{AR} \leqslant 86.8$ whilst maintaining a constant cross-sectional area, in this case, of 1.25 mm^2. For a constant cross-sectional area of channel, the aspect ratio was varied by varying both the width w_c, and height H, of the channels. For the simulation, 10^{-5} kg/s per channel of N_2 at 1.358 bar and 750 °C and 10^{-5} kg/s per channel of CO_2 at 1.338 bar and 220 °C in counter-flow were the working fluids.

Fig. 2 shows the variation of heat flux, heat transfer rate and pressure drop in each channel with the aspect ratio, AR. It is clear from the figure that as the aspect ratio of the microchannel increases there is a rapid decrease in the heat flux coupled to a rapid increase in the pressure drop. Since the heat flux, and for that matter the heat transfer coefficient, and pressure loss have opposing trends there must be a balance between the two in choosing an optimal aspect ratio. The optimal aspect ratio lies in the optimal region which is the region between the intersection of the tangents at the points of maximum and minimum curvature on the heat transfer rate and heat flux curves. This region, marked by the ellipse shown in Fig. 2, corresponds to the projection of the points A and B onto the abscissa, i.e., A' and B'. To the left of that region, even though the heat flux is high and pressure loss is low in the μHEX, by its very design (see Fig. 1), the heat transfer rate is low. On the other hand, the portion of the graph to the right of the optimal region shows a very gradual increase in heat transfer with a correspondingly high pressure loss. It stands to reason that not much would be gained in designing the heat exchanger to operate in that zone (to the right of the optimum region). It follows from the above discussion that for a given material and volume

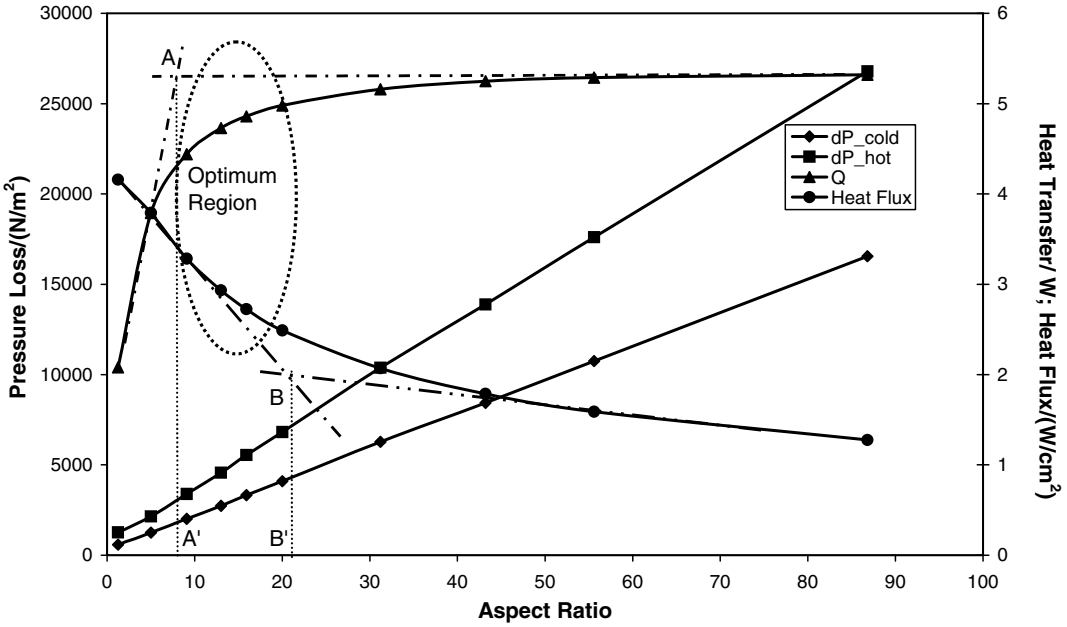

Fig. 2. Variation of pressure loss, heat transfer rate and heat flux with channel aspect ratio (constant volume).

of μHEX, the optimal dimensions of the channels could be obtained based on the choice of optimal aspect ratio which must lie within $A'B'$.

Below are shown examples of the microchannel dimensions based on aspect ratios within the marked optimum region:

(1) Optimal height = 3.38 mm, optimal width = 0.37 mm, AR = 9.1,
(2) Optimal height = 4.03 mm, optimal width = 0.31 mm, AR = 13.0,
(3) Optimal height = 4.46 mm, optimal width = 0.28 mm, AR = 15.9,
(4) Optimal height = 5.00 mm, optimal width = 0.25 mm, AR = 20.0.

3.1.2. Variable volume of microchannels

In this study, the volume of the μHEX varied but was kept within limits that define a μHEX (i.e., $1\ \mu m \leqslant d_h \leqslant 1000\ \mu m$). The flow rate of fluid (hot and cold) was kept constant for the different volume of μHEXs analyzed. Similar to Section 3.1.1 the length of the microchannels was fixed leaving the cross-sectional area as the variable. For the sake of simplicity the aspect ratio was varied by changing the height of microchannels but keeping the width constant at 0.25 mm. CFD simulations were performed by varying the aspect ratio of the microchannels in the range $5 \leqslant AR \leqslant 100$. For the analysis, 1.12×10^{-5} kg/s per channel of N_2 at 1 bar and 750 °C and 6.0×10^{-6} kg/s per channel of CO_2 at 1 bar and 220 °C in counter-flow were used as working fluids.

Fig. 3 shows the variation of heat flux, heat transfer rate and pressure drop in each channel with the aspect ratio, AR. As the aspect ratio of the microchannel increases there is a corresponding increase in the heat transfer rate up to a maximum value after which the heat transfer rate decreases. For constant mass flow rate of a fluid, a higher aspect ratio leads to a lower fluid velocity. In addition, the hydraulic diameter of the channel increases with aspect ratio. The increase in hydraulic diameter with aspect ratio combined with the attendant decrease in fluid velocity leads to lower pressure drop in the channels as is shown in the figure.

For the geometry under consideration (Fig. 1), increasing the channel aspect ratio increases the heat transfer area and consequently the transfer of heat. On the other hand, the increase in aspect ratio reduces the fluid velocity (and consequently the Reynolds number of the flow) thus leading to a lower heat transfer coefficient. Thus, there are two competing factors contributing to the transfer of heat. A point is reached when the gain in heat transfer with increasing aspect ratio is offset by the loss caused by the decrease in convective heat transfer coefficient as a result of the lower velocity and hence the Reynolds number. This effect is reflected in the curve of the heat transfer rate, Fig. 3.

The broken line in Fig. 3 marks the (optimal) aspect ratio corresponding to the maximum heat transfer rate. The portion of the figure to the left of the maximum is characterized by high heat flux as well as high pressure loss. On the other hand, the portion to the right of the optimal aspect ratio shows a very gradual decrease in heat transfer whereas the aspect ratio and hence the volume of μHEX increases. Thus, operating in the region to the right of the maximum point would tremendously reduce the energy density of a μHEX.

It must be emphasized that the graphs shown in Figs. 2 and 3 are case-specific and the designer of a μHEX must

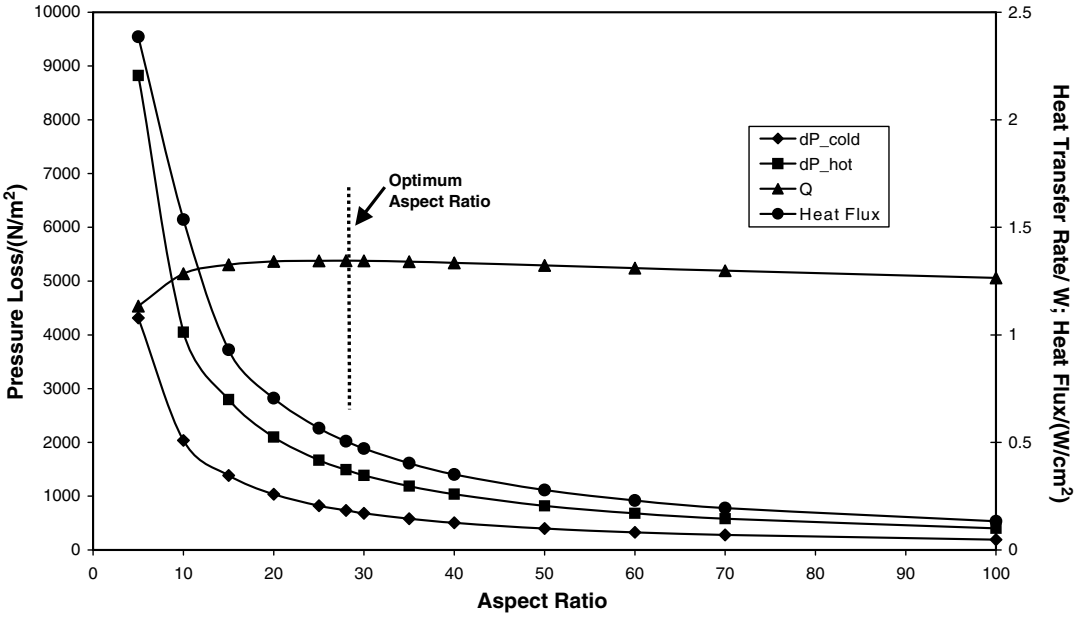

Fig. 3. Variation of pressure loss, heat transfer rate and heat flux with channel aspect ratio (variable volume).

first obtain the characteristic curves for the type of heat exchanger under consideration. Based on the characteristics and the design constraints an optimal AR and, subsequently, the optimal dimensions could be obtained.

3.1.3. Optimal dimensions

This section deals with the approach used in calculating the optimal geometric parameters of the channels of a μHEX when the volume of the μHEX is not fixed by design considerations (Section 3.1.2). Associated with any known optimal aspect ratio, AR_{opt}, is an infinite number of pairs of channel height and width.

In calculating the optimal dimensions of the microchannel based on the chosen AR the analytical approach of Samalam [12] was used. Though derived for microchannels designed for cooling electronic chips, a thorough investigation of the analysis revealed that the approach could be applied to the type of μHEXs discussed here.

According to Samalam, for low aspect ratios, $AR \leqslant 10$, the optimal dimensions of a microchannel are given by

$$w_c = b, \quad \text{and} \quad w_s = H\sqrt{\frac{k_f Nu}{6k_s}},$$

$$\text{where } b^4 = \frac{12\mu k_f Nu l^2}{\rho c_p \Delta P}. \tag{5}$$

The above is valid for

$$\frac{H}{b} \ll \pi^2 \left[\frac{k_s}{6k_f Nu}\right]^{1/2}. \tag{6}$$

For high aspect ratios, $AR > 10$

$$w_s = \frac{w_c}{2}, \quad \text{and} \quad w_c = \frac{2^{1/6} b^{4/3}}{\alpha^{1/6} H^{1/3}}, \quad \text{where } \alpha = \frac{k_f Nu}{k_s}. \tag{7}$$

Eqs. (7) are valid for

$$\frac{H}{b} \gg \frac{\pi^{3/4}}{(2\alpha)^{1/4}}. \tag{8}$$

The steps followed for calculating the optimal geometric parameters are discussed in Table 1. Since optimal geometric parameters are dependent on the thermophysical properties of fluids, it is obvious that a μHEX operating with two different fluids or even with the same fluid at different temperatures will have different optimal dimensions for the channels transporting both fluids.

For the purpose of illustration the optimal geometrical parameters of a μHEX based on the operating conditions provided in this subsection are calculated. In Fig. 3, the optimal aspect ratio, AR_{opt}, corresponding to the maximum heat transfer rate is 28. The task of determining the optimal dimensions from the infinite set of all possible pairs, (H, w_c), is accomplished by using Eq. (7) (for $AR_{opt} > 10$). Using average values based on inlet and

Table 1
Optimization steps

$AR_{opt} \leqslant 10$	$AR_{opt} > 10$
Determine *Nu* based on fluid properties	Determine *Nu* based on fluid properties
Fix allowable pressure loss ΔP	Fix allowable pressure loss ΔP
Decide on length of channels l based on space limitation	Decide on length of channels l based on space limitation
Calculate b from Eq. (5)	Calculate b from Eq. (5)
From Eq. (5), $w_c = b$	Calculate α form Eq. (7)
From Eq. (4), $H = w_c AR_{opt}$	From Eqs. (4) and (7), $w_c = \frac{2^{1/8} b}{\alpha^{1/8} AR_{opt}^{1.4}}$
From Eq. (5), $w_s = w_c AR_{opt}\sqrt{\frac{k_f Nu}{6k_s}}$	From Eq. (4), $H = w_c AR_{opt}$
Check the validity condition (Eq. (6))	From Eq. (7), $w_s = \frac{w_c}{2}$
	Check the validity condition (Eq. (8))

outlet temperatures for the fluid properties appearing in Eqs. (5)–(8), the dimensions of the hot and cold side channels were calculated as follows:

$$\text{Hot side:}\quad H = 14.80\,\text{mm},\quad w = 0.53\,\text{mm},\quad s = 0.26\,\text{mm},$$
$$\text{Cold side:}\quad H = 11.76\,\text{mm},\quad w = 0.42\,\text{mm},\quad s = 0.21\,\text{mm}.$$

For the geometry under consideration it would not be feasible from a design point to have different dimensions for the hot- and cold-side microchannels. Further numerical simulations revealed that better results were achieved when the cold-side dimensions were used for all channels.

The performance of three μHEXs having the same aspect ratio was compared with a μHEX optimized according to the procedure described in this section. In Table 2 the dimensions, heat transfer rate and pressure loss in all four μHEXs are provided. A close examination of the results puts the performance of the optimized μHEX above the pack.

Table 2
Comparison between optimized and non-optimized μHEXs

	H (mm)	w (mm)	s (mm)	AR	Q (W)	ΔP_{cold} (Pa)	ΔP_{hot} (Pa)
Optimized HEX	11.76	0.42	0.21	28	3.59	446	1333
HEX1	5.88	0.21	0.105	28	0.790	1503.0	5132
HEX2	7.84	0.28	0.140	28	0.747	425.0	1565
HEX3	12.88	0.46	0.231	28	0.752	57.55	210

3.2. Optimization with multiple criteria

In μHEXs there are several usually competing properties that must be taken into account, e.g., the minimization of the pressure drop and the maximization of the heat flux. In the second approach, we will, therefore, treat the design of μHEX as a multi-objective optimization problem. Here, the target is a set of solutions called the Pareto front of a multi-objective optimization (MOO) problem. The definition of the Pareto front will be provided in Section 3.2.1. To tackle MOO problems, we will use evolutionary algorithms. Besides the known strength of evolutionary computation, like robustness and the possibility to escape local optima, the population based approach of evolutionary methods is particularly suitable for MOO problems because the target is to identify a set of solutions instead of one optimal solution.

3.2.1. Evolutionary multi-objective optimization

In this section, we will shortly introduce the main principles of evolutionary algorithms and outline the multi-objective optimization method [29,30].

Evolutionary algorithms (EAs) are direct pseudo-stochastic search methods which mimic the principles of Neo-Darwinian evolution. A population of possible solutions (e.g., a vector[2] of continuous parameters, the objective variables, describing a μHEX geometry) is adapted to solve a given problem (e.g., minimization of pressure drop) over several generations. The adaptation occurs by varying these solutions in the population and by selecting the best solutions for the next generation. The variations can be classified as purely stochastic (usually called mutation) and combinatoric/stochastic (usually called recombination or in the context of genetic algorithms crossover). Schematically the evolution cycle is shown in Fig. 4(a), formally, an evolutionary algorithm can be described by Fig. 4(b).

In multi-objective optimization, several competing objectives exist. As discussed in Section 3.1, this is the case for μHEX optimization. There are different ways to deal with MOO problems. One can aggregate (mostly linearly) all objectives and render the problem single objective. The drawback of this approach is that the choice of the weights is usually arbitrary. Alternatively, one can determine all solutions for which no solution exists which is better in all objectives. These solutions are called *non-dominated* and the set of all non-dominated solutions is referred to as the *Pareto front*, see Fig. 5.

The second approach leaves maximum freedom to the designer since objectives are not weighted prior to the optimization but instead the most appropriate solution is chosen from the Pareto front. However, it is also the computationally most demanding approach considered in this work. Since EAs inherently operate on a set of solutions, the so-called *population*, they are particularly suitable to find and represent the Pareto front.

In this paper, we will apply the NSGA-II [31,32] to identify the Pareto front, which is widely recognized as one of the most powerful MOO algorithms. The Pareto front for the NSGA-II is represented in the final population.

The NSGA-II (a fast and elitist non-dominated sorting genetic algorithm) proposed by Deb et al. [31,32] is a multi-objective extension of the standard genetic algorithm with binary/gray coding. In the context of NSGA-II, a floating point representation can also be used. Whether a binary/gray coding is more or less suitable than a floating point representation is especially for multi-objective optimization difficult to decide and certainly depends on the problem. Some preliminary research indicates that the best choice would be a hybrid representation, so that a switching mechanism is able to choose the current optimal representation dependent on the search space, see [33].

In our approach, the real parameter values are binary encoded and the standard crossover and mutation method are used for the variation of solutions. The selection method is based on two measures which are specific to MOO. The above introduced principle of non-domination is used as well as a measure that aims at maintaining diversity and "spread" of the solutions that are to represent the Pareto front. Details of the algorithm can be found in [31,32].

[2] Note, that this vector is also called chromosome in imitation of evolutionary biology.

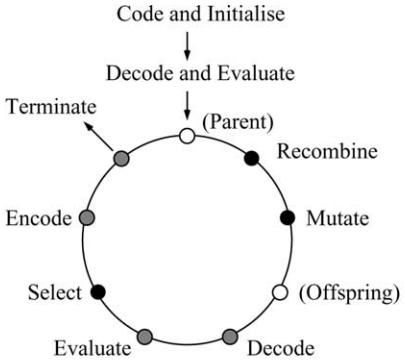

(a)

Evolutionary Algorithms		Nomenclature	
$t := 0;$		$P_g(t)$	Genotype population, Generation t
Initialize $P_g(0) := \{g_1(0), ..., g_\mu(0)\}$		$P_p(t)$	Phenotype population, Generation t
Decode and Evaluate $P_g(0) : \Phi(c_{\theta_c}^{-1}(P_g(0)))$		Q	Additional set of individuals, e.g. $P_p(t)$
Do		$g_1(t)$	Genotype of the first individual
Recombine	$P'_g(t) := r_{\theta_r}(P_g(t))$	Φ	Fitness function
Mutate	$P''_g(t) := m_{\theta_m}(P'_g(t))$	μ, λ	Population size (parents, offspring)
Decode	$P''_p(t) := c_{\theta_c}^{-1}(P''_g(t))$	r_{θ_r}	Recombination operator
Evaluate	$\Phi(P''_p(t))$	m_{θ_m}	Mutation operator
Select	$P_p(t+1) := s_{\theta_s}(P''_p(t) \bigcup Q)$	$c_{\theta_c}, s_{\theta_s}$	Coding and Selection operator
Code	$P_g(t+1) := c_{\theta_c}(P_p(t+1))$		
$t := t+1$			
Until stop			

(b)

Fig. 4. Flow of evolutionary computation. First, a population is generated randomly and evaluated. This becomes the parent population, from which offspring are generated using recombination (crossover) and mutation. From the evaluated offspring population, promising individuals are selected to become the next parent population. This iteration is repeated until a certain termination condition is met. (a) Evolution cycle, (b) formal description of evolutionary algorithms.

3.2.2. Optimization environment

3.2.2.1. Design parameters. The goal is to find the optimal shape of the separator that simultaneously maximizes heat transfer and minimizes pressure drop in the micro heat exchanger. To simplify this problem, the height H and the length l in Fig. 1 are fixed. In addition, the cross-sectional area of the flow passages are also kept constant. The shape of the separator is represented by two *Non-Uniform Rational B-splines* (*NURBS*) [34]. The *B*-spline representation consists of a number of control points, which define the control polygon of the shape, a number of knot points and a number of weights. We keep the knot points and the weights[3] constant and only vary the control points. In this work, we use 10 control points. We specify one end wall of the separator with the spline and define the second wall using the constant thickness of the separator.[4]

3.2.2.2. Objective functions. The objectives of the optimization are to maximize the heat transfer and to minimize the

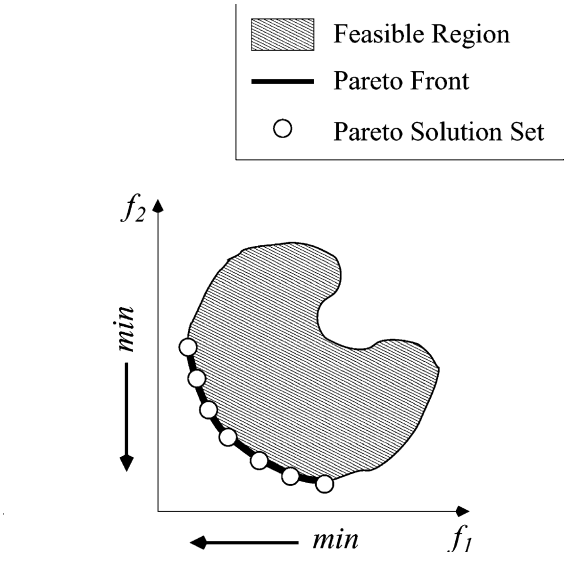

Fig. 5. Pareto front and Pareto solution set. Here, two objectives to be minimized are assumed. The bold curve is the Pareto front that is the solution of multi-objective optimization.

[3] The weights are set to one.

[4] To keep the cross-sectional area of the flow passages constant, their width are modified according to the shape of the separators.

pressure drop in the hot gas channel and in the cold gas channel [35,36]. To render both problems minimization problems, we multiply the heat transfer by −1. Therefore, we get the following two objectives:

$$f_1(\vec{x}) = -Q, \qquad f_2(\vec{x}) = \Delta P_h + \Delta P_c, \tag{9}$$

where Q is the heat transfer and ΔP_h and ΔP_c are the pressure drops in the hot gas channel and in the cold gas channel, respectively.

3.2.2.3. Calculation constraints and mesh generation. The hot gas consists of a mixture of methane, hydrogen, steam, carbon monoxide, carbon dioxide and nitrogen; the cold gas is a mixture of methane, steam, oxygen and nitrogen. The heat transfer with the surroundings is assumed adiabatic. In this problem the exchange of heat between alternate channels is across the separator.

The inlet conditions for the gases are as follows:

Flow rate (g/s) = 3.06 (for hot gas and cold gas),
Inlet temperature (°C) = 750, 220 (for hot gas, cold gas),
Inlet pressure (kPa gauge) = 34.5, 36.5 (for hot gas, cold gas),
Allowable pressure drop (kPa) = 1.0 (for hot gas and cold gas).

For the optimization the CFD-ACE+ program had to be interfaced with the multi-objective evolutionary algorithms. The details of this interface are explained in [35,36].

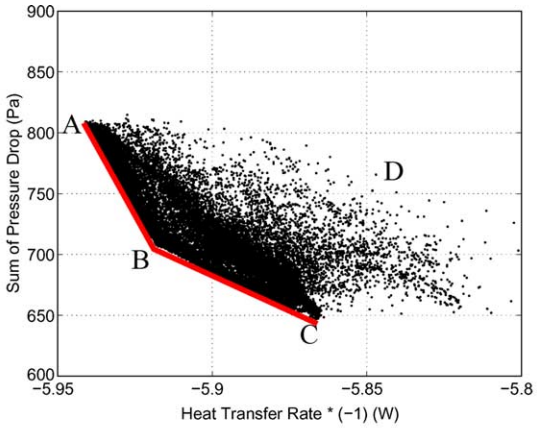

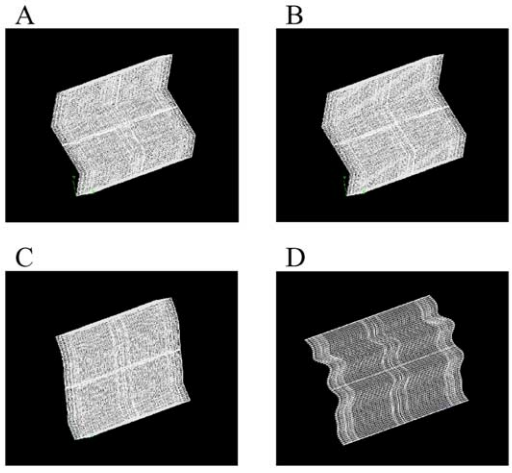

Point	$HTR(W)$	$\Delta P_h(Pa)$	$\Delta P_c(Pa)$	Heat Flux $(10^{-8}W/m^2)$
A	5.941	458.6	350.4	1.106
B	5.918	386.6	321.1	1.101
C	5.866	357.5	289.4	1.161
D	5.840	431.6	343.1	1.031

Fig. 6. Final result by NSGA-II (after one-month calculation). In the upper figure, all evaluated individuals are shown. One point corresponds to one design of μHEX. The gray (red in the web version) line ($\overline{AB}, \overline{CD}$) shows the estimated Pareto curve. Four representative shapes A, B, C and D are shown together with their values for heat transfer rate (HTR), pressure drops ΔP_h, ΔP_c and the heat flux.

The auto-mesh generator for a structural grid from CFD-ACE+ was used in the optimization. In order to handle poorly generated meshes or errors in the spline representation (e.g., loops), individuals for which the flow solver was unable to satisfy a preset convergence criterion were removed from the population.

3.2.3. Results of NSGA-II

The parameters in NSGA-II are set as follows:

Number of individuals = 100,
Number of bits per one floating value = 20,
Range of floating value in Y-direction = $[-0.25H, 0.25H]$ (accuracy = $0.5H \times 2^{-20} \approx 0.5H \times 10^{-6}$),
Range of floating value in Z-direction = $[0, H]$ (accuracy = $H \times 2^{-20} \approx H \times 10^{-6}$),
Maximum generations = 500,
Crossover/rate = One point crossover/0.9,
Mutation/rate = Bit flip/0.05.

The result of the optimization study is shown in Fig. 6 with each point representing a solution. The figure shows all evaluated solutions and the estimated Pareto curve as red (gray) lines. The shapes of three representative solutions (together with their values for heat transfer rate (HTR), pressure drops ΔP_h, ΔP_c and heat flux) on the Pareto front and one solution far away from the Pareto front are shown. The results clearly reveal the conflict between the two objectives, the heat transfer and the pressure drop. Any geometrical change that increases the heat transfer rate and for that matter the heat flux leads to an increase in the pressure drop and vice versa. Thus, it is evident that multi-objective optimization techniques are necessary for the optimization of the μHEX. We also observe that the Pareto front consists of two parts, i.e., the lines $\overline{AB}$ and $\overline{BC}$. One would expect that the shapes of the μHEX on both parts are different, however they are not. The reason for the bend in the Pareto front at point B remains unclear and will be the subject of further studies.

All shapes on the Pareto front are (at least topologically, e.g., with regard to their periodicity[5]) strikingly similar. Theoretically, the spline with 10 control points can represent curves with higher periodicity than the ones obtained. A natural question is why all geometries that are visited by the optimization algorithm have relatively similar shape and low periodicity. Although the data obtained from our experiments is not sufficient to give a definite answer to this question, we can offer two hypotheses: (1) although theoretically possible, the practical realization of shapes with higher periodicity by splines with 10 control points is difficult and requires correlated changes of the control points which are difficult to achieve for stochastic optimization methods like evolutionary algorithms; (2) the ratio of the number of geometries with good performance to all geometries becomes smaller with increasing periodicity, i.e., even though higher periodicity might lead to better solutions, they are harder to find. There is some evidence for both suggestions. In particular, the first one seems intuitively correct, although for a robust optimization technique it should still be possible to realize splines with higher periodicity. The fact that in Fig. 6, a poorly performing solution (D) has a shape with higher periodicity might point in the direction of the second hypothesis. Some first results with a different representation have been obtained in [35]. A combination of both representations might allow to answer the question on the influence of the representation on the optimization result more comprehensively.

[5] We use the term periodicity in a rather intuitive way. Mathematically, a function $w(t)$ is periodic, if $w(t) = w(t + T)$ with the period $T = v^{-1}$ and frequency v. Higher periodicity here implies higher frequency. However, in our intuitive use of periodicity, we describe end walls which are similar to e.g., a sine or a saw-tooth pattern with long or short period.

4. Conclusion

It has been demonstrated in this paper that the performance of micro heat exchangers depends on the operating conditions and aspect ratio of the microchannels that make up the flow passages. Using the simpler approach we were able to optimize the dimensions of a rectangular microchannel. The optimized dimensions presented in Section 3.1.3 lead to higher heat flux and heat transfer rates.

With the more advanced approach, we discussed the problem of the optimal shape of micro heat exchangers in the context of multi-objective evolutionary optimization. Here we introduced two objectives, the heat transfer and the sum of pressure drops. We applied NSGA-II (Non-dominated Sorting Genetic Algorithm) to identify the Pareto front that is the trade-off curve between the two objectives for this problem. Starting with a rectangular shape, our optimization tool was able to generate different geometries. The optimum geometry obtained with this method yielded heat fluxes greater than those obtained with the less advanced approach.

There are several conclusions which can be drawn from our studies:

- The performance of micro heat exchangers with respect to the measures that we analyzed in this paper clearly depends on their geometry.
- There is a trade-off between minimal pressure drop and maximal heat transfer. This trade-off is made visible by the Pareto curves that we obtained in our optimization experiments.
- The dependence of the performance on the geometry is non-trivial, i.e., simply increasing the periodicity does not necessarily lead to better solutions.

Results that have been published previously in the literature gave higher heat flux values than those obtained in

this paper. Higher heat flux and heat rate values could be easily obtained by changing the operating conditions and the type of fluid. However, the target of this paper is to analyze the intrinsic interaction between performance and design or shape of micro heat exchangers on the background of different optimization techniques. Pareto curves of the optimization exhibit some interesting dependencies. It will be the target of future work to confirm these dependencies by real experiments and to get a more in-depth understanding of the relation between the periodicity of the geometry and the performance of the micro heat exchanger both with respect to minimal pressure drop and maximal heat transfer.

Acknowledgements

The authors would like to thank E. Körner, A. Richter, L. Freund and T. Arima for their kind and continuous support. Mr. Peters of CFD Research Corporation is acknowledged for his flexibility regarding the parallel interface between CFD-ACE+ and our optimization software. We also thank K. Shibata (Wave Front Co., Ltd.) for his support to build up the connection between the CFD part and the optimization.

References

[1] D.B. Tuckerman, R.F.W. Pease, High-performance heat sinking for VSLI, IEEE Electron Dev. 2 (1981) 126–129.
[2] J. Pfahler, J. Harley, H.H. Bau, J. Zemel, Liquid and gas transport in small channels, in: D. Choi et al. (Ed.), ASME-DSC 19, 1990, pp. 149–157.
[3] J. Pfahler, J. Harley, H.H. Bau, J. Zemel, Gas and liquid flow in small channels, in: D. Choi et al. (Ed.), Micromechanical Sensors, Actuators and Systems, ASME-DSC 32, 1991, pp. 49–60.
[4] X.F. Peng, G.P. Peterson, B.X. Wang, Frictional flow characteristics of water flowing through rectangular microchannels, Exp. Heat Transfer 7 (1994) 249–264.
[5] X.F. Peng, G.P. Peterson, The effect of thermofluid and geometrical parameters on convection of liquids through rectangular channels, Int. J. Heat Mass Transfer 38 (4) (1995) 755–758.
[6] X.F. Peng, G.P. Peterson, Convective heat transfer and flow friction for water flow in microchannel structures, Int. J. Heat Mass Transfer 39 (12) (1996) 2599–2608.
[7] B.X. Wang, X.F. Peng, Experimental investigation on liquid forced convection heat transfer through microchannels, Int. J. Heat Mass Transfer 37 (1994) 73–82.
[8] T.M. Harms, M.J. Kazmierczak, F.M. Gerner, Developing convective heat transfer in rectangular microchannels, Int. J. Heat Fluid Flow 20 (1999) 149–157.
[9] H.J. Park, S.Y. Son, M.C. Choi, G. Lim, I.S. Song, J.J. Pak, Temperature-dependent property effects on laminar flow characteristics in a rectangular microchannel, in: Proceedings of ASME IMECE MEMS-23865, 2001.
[10] W. Qu, I. Mudawar, Experimental and numerical study of pressure drop and heat transfer in a single-phase micro-channel heat sink, Int. J. Heat Mass Transfer 45 (2002) 2549–2565.
[11] M.N. Sabry, Scale effects on fluid flow and heat transfer in microchannels, IEEE Trans. Compon. Packaging Technol. 23 (3) (2000) 562–567.
[12] V.K. Samalam, Convective heat transfer in microchannels, J. Electron. Mater. 18 (5) (1989) 611–617.
[13] R.W. Knight, J.S. Goodling, D.J. Hall, Optimal thermal design of forced convection heat sinks—analytical, J. Electron. Packaging 113 (1991) 313–321.
[14] R.W. Knight, J.S. Goodling, D.J. Hall, R.C. Jaeger, Heat sink optimization with application to microchannels, IEEE Trans. Compon. Packaging Technol. 15 (5) (1992) 832–842.
[15] J.B. Aparecido, R.M. Cotta, Thermally developing laminar flow inside rectangular ducts, Int. J. Heat Mass Transfer 33 (2) (1990) 341–347.
[16] X. Wei, Y. Joshi, Optimization of stacked micro-channel heat sinks for micro-electronic cooling, Int. Soc. Conf. Therm. Phenomena (2002) 441–448.
[17] C.P. Tso, S.P. Mahulikar, The use of the Brinkman number for single phase forced convective heat transfer in microchannels, Int. J. Heat Mass Transfer 41 (12) (1998) 1759–1769.
[18] J.M. Li, B.X. Wang, X.F. Peng, 'Wall-adjacent layer' analysis for developed-flow laminar heat transfer of gases in microchannels, Int. J. Heat Mass Transfer 43 (2000) 839–847.
[19] G. Tunc, Y. Bayazitoglu, Heat transfer in rectangular microchannels, Int. J. Heat Mass Transfer 45 (2002) 765–773.
[20] S.T. Poh, E.Y.K. Ng, Heat transfer and flow issues in manifold microchannel heat sinks: a CFD approach, in: IEEE/CPMT Electron. Packag. Technol. Conf., 1998, pp. 246–250.
[21] E.Y.K. Ng, S.T. Poh, CFD Analysis of double-layer microchannel conjugate parallel liquid flows with electric double-layer effects, Numer. Heat Transfer Part A 40 (2001) 735–749.
[22] A.G. Fedorov, R. Viskanta, Three-dimensional conjugate heat transfer in the microchannel heat sink for electronic packaging, Int. J. Heat Mass Transfer 43 (2000) 399–415.
[23] K.K. Ambatipudi, M.M. Rahman, Analysis of conjugate heat transfer in microchannel heat sinks, Numer. Heat Transfer Part A 37 (2000) 711–731.
[24] H.H. Bau, Optimization of conduits' shape in microheat exchangers, Int. J. Heat Mass Transfer 41 (1998) 2117–2723.
[25] S.V. Patankar, D.B. Spalding, A calculation procedure for heat, mass and momentum transfer in three-dimensional parabolic flows, Int. J. Heat Mass Transfer 15 (1972) 1787–1806.
[26] J.P. Van Doormaal, G.D. Raithby, Enhancements of the SIMPLE method for predicting incompressible flows, Numer. Heat Transfer 7 (1984) 147–163.
[27] G. Lonsdale, An algebraic multigrid solver for the Navier–Stokes equations on unstructured meshes, Int. J. Numer. Methods Heat Fluid Flow 3 (1993) 3–14.
[28] CFD-ACE+ Theory Manual, Version 2002, CFD Research Corporation, 215 Wynn Drive, Huntsville, AL 35805, 2002.
[29] K. Deb, Multi-objective Optimization Using Evolutionary Algorithms, John Wiley & Sons, 2001.
[30] C.A. Coello Coello, D.A. Van Veldhuizen, G.B. Lamont, Evolutionary Algorithms for Solving Multi-objective Problems, Kluwer Academic Publishers, 2001.
[31] K. Deb, S. Agrawal, A. Pratap, T. Meyarivan, A fast elitist non-dominated sorting genetic algorithm for multi-objective optimization: NSGA-II, in: Proceedings of the Parallel Problem Solving from Nature PPSN VI, 2000, pp. 849–858.
[32] K. Deb, A. Pratap, S. Agarwal, T. Meyarivan, A fast and elitist multiobjective genetic algorithm: NSGA-II, IEEE Trans. Evol. Comput. 6 (2) (2002) 182–197.
[33] T. Okabe, Y. Jin, B. Sendhoff, Evolutionary multi-objective optimisation with a hybrid representation, in: Proceedings of the IEEE Congress on Evolutionary Computation CEC, 2003, pp. 2262–2269.
[34] L. Piegl, W. Tiller, The NURBS Book, second ed., Springer, 1997.
[35] T. Okabe, K. Foli, M. Olhofer, Y. Jin, B. Sendhoff, Comparative studies on micro heat exchanger optimisation, in: Proceedings of the IEEE Congress on Evolutionary Computation CEC, 2003, pp. 647–654.
[36] T. Okabe, Evolutionary Multi-objective Optimization—On the Distribution of Offspring in Parameter and Fitness Space, Shaker Verlag, 2004, ISBN 3-8322-2904-3.